Tunable Solvation Effects on the Size-Selective Fractionation of Metal Nanoparticles in CO_2 Gas-Expanded Solvents

Madhu Anand, M. Chandler McLeod, Philip W. Bell, and Christopher B. Roberts*

Department of Chemical Engineering, Auburn University, Auburn, Alabama 36849

Received: August 19, 2005; In Final Form: October 5, 2005

This paper presents an environmentally friendly, inexpensive, rapid, and efficient process for size-selective fractionation of polydisperse metal nanoparticle dispersions into multiple narrow size populations. The dispersibility of ligand-stabilized silver and gold nanoparticles is controlled by altering the ligand tails−solvent interaction (solvation) by the addition of carbon dioxide (CO_2) gas as an antisolvent, thereby tailoring the bulk solvent strength. This is accomplished by adjusting the CO_2 pressure over the liquid, resulting in a simple means to tune the nanoparticle precipitation by size. This study also details the influence of various factors on the size-separation process, such as the types of metal, ligand, and solvent, as well as the use of recursive fractionation and the time allowed for settling during each fractionation step. The pressure range required for the precipitation process is the same for both the silver and gold particles capped with dodecanethiol ligands. A change in ligand or solvent length has an effect on the interaction between the solvent and the ligand tails and therefore the pressure range required for precipitation. Stronger interactions between solvent and ligand tails require greater CO_2 pressure to precipitate the particles. Temperature is another variable that impacts the dispersibility of the nanoparticles through changes in the density and the mole fraction of CO_2 in the gas-expanded liquids. Recursive fractionation for a given system within a particular pressure range (solvent strength) further reduces the polydispersity of the fraction obtained within that pressure range. Specifically, this work utilizes the highly tunable solvent properties of organic/CO_2 solvent mixtures to selectively size-separate dispersions of polydisperse nanoparticles (2 to 12 nm) into more monodisperse fractions (±2 nm). In addition to providing efficient separation of the particles, this process also allows all of the solvent and antisolvent to be recovered, thereby rendering it a green solvent process.

Introduction

Nanoparticle-based technologies take advantage of the fact that materials built from particles less than a critical length[1] display unique chemical and physical properties. These properties depend heavily on the size, shape, and composition of the nanoparticles. The size-dependent properties of nanoparticles allows one to engineer them to have a specific function such as in catalysts,[2−4] quantum dots for optical properties,[5,6] and medical applications.[7] The preparation of monodisperse metal particles is also necessary to study the effects of size on their novel applications including size-dependent conduction of electrons in Ag nanoparticles[8] and size-dependent oxidation with Au catalysts.[9,10] Moreover, monodisperse nanoparticles are also critical in the production of high-quality ordered arrays and ordered thin films.[11−14]

There are numerous methods to produce metal nanoparticles, including simple solution-based techniques such as reverse micelle synthesis[15,16] and two-phase arrested precipitation methods.[17] While these particular solution-based techniques are attractive due to their simplicity, they often result in the synthesis of particle sizes with a wide size range (e.g., 2 to 12 nm). As such, post-synthesis processing is required to further refine the size distribution to the desired narrow monodisperse range. Herein we will use the relaxed definition of monodisperse particles as being samples that have standard deviation, σ, of diameter less than 5%[18] to 10%. A variety of post-synthesis techniques have been developed to narrow size distributions including the use of liquid antisolvents[14,19,20] to selectively control precipitation, isoelectric focusing electrophoresis (IEF),[21] and chromatography techniques.[22] As an example, Sigman et al.[20] used ethanol as an antisolvent and centrifugation to size-selectively precipitate and separate a polydisperse dispersion of silver nanoparticles capped with dodecanethiol ligands into monodisperse particle fractions.

In these liquid antisolvent nanoparticle precipitation techniques, ligand-capped particles are first dispersed in solution where the interaction between the solvent and the ligand tails provides enough repulsive force to overcome the inherent van der Waals attraction between the particles that would otherwise result in agglomeration and precipitation. Through the addition of an antisolvent, the resultant poorer solvent mixture interacts less with the ligand tails than did the pure solvent, thereby reducing the ability of the solvent/antisolvent mixture to disperse the particles. Larger particles possess greater interparticle van der Waals attractions and therefore precipitate first upon worsening solvent conditions followed by subsequent precipitation of the smaller sized particles with further addition of antisolvent. Applying centrifugation then provides an external force to accelerate the precipitation process. Repetition of this antisolvent/centrifugation method on the separated particles can result in narrow particle size distributions, $\sigma < 5\%$; however, the whole process is both solvent and time intensive. It is also difficult to obtain an a priori desired particle size through this

* Address correspondence to this author. E-mail: croberts@eng.auburn.edu. Phone: (334) 844-2036. Fax: (334) 844-2063.

10.1021/jp0547008 CCC: $30.25
Published on Web 11/12/2005

separation process in a repeatable manner simply by changing the composition of the liquid antisolvent/solvent pair. To overcome this limitation, and to provide improved control over size-selective precipitation, McLeod et al.[23] developed an antisolvent precipitation technique based on the pressure tunable solvent properties of gas-expanded liquid mixtures (liquid solvents pressurized with CO_2) as described later in this paper.

Research in the area of nanoparticle processing using compressed and supercritical fluid solvents has shown that the pressure and temperature tunable solvent properties in these systems provide a means to control the size of nanoparticles that can be synthesized and/or dispersed.[24−27] Shah et al. demonstrated the size-selective dispersion of dodecanethiol coated nanoparticles in supercritical ethane by density tuning.[28] They illustrated that with the change in solvent density, the dispersable particle size could be adjusted where the largest particle sizes were dispersed at the highest pressure. However, ethane is a feeble solvent and very high pressures of around 414 bar were required to disperse particles of only 3.7 nm in size. Efficient solvent-based separation techniques for a wide range of nanoparticle sizes would require better solvent strength than these supercritical solvents are able to provide at significantly lower pressures.

Gas-expanded liquid systems, on the other hand, provide a wide range of solvent properties (from liquid-like to gas-like) that are widely tunable with simple adjustments in gas pressure thereby providing further opportunity for nanoparticle precipitation and separation.[23] For example, Han and co-workers recently precipitated nanoparticles from AOT reverse micelles in liquid isooctane using pressurized CO_2 as an antisolvent.[29−31] This antisolvent effect with CO_2 is available because compressed gases such as CO_2 dissolve into organic liquids and expand the liquid volume significantly while also altering the liquid's solvation characteristics. These pressurized liquid solutions of organic solvent and CO_2 mixtures are commonly referred to as gas-expanded liquids (GELs). Among their many applications, GELs have been used as tunable reaction media,[32−34] as adjustable solvents for separations,[35−38] in the switching of fluorous compound solubilities,[39] and in gas antisolvent (GAS) precipitation techniques for organic and polymer microparticle formation.[40] CO_2 is an excellent choice in these gas-expanded liquids as it is a very weak solvent even at high pressures[41] and has no dipole moment and very low refractive index.[24] As such, the solvent strength of CO_2-expanded organic liquid solutions can be varied from that of the pure organic to that of liquid CO_2 at pressures below the vapor pressure of CO_2.

McLeod et al.[23] utilized the highly tunable solvent properties of CO_2-expanded organic solvents to size-selectively precipitate and separate ligand-stabilized metal nanoparticle dispersions into narrow distributions through fine adjustments in CO_2 pressure. By pressurizing an organic solution with CO_2, ligand-stabilized nanoparticles were size-selectively precipitated within a novel apparatus that confined the particles to specified locations on a surface allowing their separation. Accordingly, the solvent strength of the medium was tuned through successive CO_2 pressurization to provide sequential precipitation of increasingly smaller particles. A novel spiral tube apparatus was developed for separating polydisperse silver nanoparticles into different fractions of uniform sizes by regulating the CO_2 pressure[23] and therefore altering the liquid's solvation of the particle ligand tails. The advantage of this apparatus is that it separates a polydisperse solution of nanoparticles into fairly monodisperse fractions in one contiguous process. This method has a number of advantages compared to traditional liquid-based size-selection methods and can be applied to a broader range of particle sizes as compared to SCF CO_2 particle processing while operating at much lower pressures. This method also avoids the use of expensive and environmentally persistent fluorinated molecules commonly used in SCF processing, while simultaneously allowing for the separation of particles from a minimum amount of organic liquid. These characteristics make it a green solvent process.

In this paper, a detailed study was performed to examine the factors influencing this nanoparticle size-separation process with use of CO_2 as antisolvent. Variations in ligand−solvent interactions were examined to demonstrate the effects of solvent strength and thiol length on the CO_2 pressure range required for particle size separation. The effect of temperature on this pressure range for precipitation was also studied. Recursive fractionation on particles collected at a given pressure range was performed to show that multiple fractionations further improve the CO_2 antisolvent size-separation process, just as is observed in traditional liquid antisolvent processes.

Experimental Section

Materials. Silver nitrate (99.8% purity)($AgNO_3$) was obtained from Acros. Hydrogen tetrachloroaurate trihydrate (99.9%) ($HAuCl_4 \cdot 3H_2O$), tetraoctylammonium bromide (98%), chloroform (99.8%), sodium borohydride (99%), dodecanethiol (98%), hexanethiol (95%), octanethiol (98.5%), tetradecanethiol (98%), hexane (99%), cyclohexane (99.5%), octane (99%), and heptane (99%) were obtained from Aldrich chemical Co. Pentane (99.6%), toluene (99%), and deionized water (D-H_2O) were obtained from Fisher. Ethanol (200 proof) was obtained from Florida Distillers. Carbon dioxide (SFC/SFE grade) was obtained from Airgas. All chemicals were used as supplied.

Nanoparticle Synthesis. Ligand-stabilized silver and gold nanoparticles were synthesized by the two-phase arrested precipitation method as developed by Brust et al.[17]

In short, a solution of 0.19 g of $AgNO_3$ in 36 mL of D-H_2O was mixed with an organic solution of 2.7 g of tetraoctylammonium bromide in 24.5 mL of chloroform. The mixture was stirred for 1 h, the aqueous phase was removed, and then 240 μL of dodecanethiol was added. A solution of 0.5 g of $NaBH_4$ in 30 mL of D-H_2O was added as a reducing agent after the mixture was stirred for 5−10 min. The mixture was then stirred for 4−12 h before discarding the aqueous phase. In addition to dodecanethiol, other thiols were used to examine the effect of thiol length on the size-separation process. In each case, the mole percentage of thiol added was the same as that of the dodecanethiol described above. Gold nanoparticles were synthesized by replacing 0.19 g of AgNO3 with 0.38 g of hydrogen tetrachloroaurate trihydrate ($HAuCl_4 \cdot 3H_2O$), replacing chloroform with toluene, and adding thiol after 4−12 h of stirring.

Once the thiol-coated metal particle dispersion was formed, ethanol was added as antisolvent. The dispersion of nanoparticles in the solvent/antisolvent mixture was then centrifuged (Fisher Centrific Model 228) to precipitate out the metallic nanoparticles. The particles were again washed with ethanol and centrifuged to remove any unbound ligands. This process of washing with ethanol was repeated 3 times to remove the phase-transfer catalyst. The particles were then dispersed in hexane by sonication (Fisher). The remaining dispersion of nanoparticles in hexane was used for further experimentation.

UV−visible Absorbance Spectroscopy. The UV−visible absorbance spectrum of the particle dispersions in both neat solvent and the CO_2-expanded solvents was measured in a high-pressure view cell with a Varian 300E spectrophotometer to

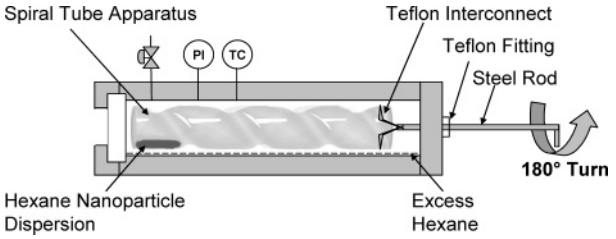

Figure 1. Nanoparticle size-selection apparatus enclosed in a high-pressure vessel shows a loading of a hexane nanoparticle dispersion. Excess hexane was loaded to saturate the high-pressure vessel with hexane vapor. A teflon fitting allows the steel rod to enter into the vessel and maintains the high-pressure seal while turning the steel rod 180°, which rotates the spiral tube with the help of the Teflon interconnect. PI and TC stand for pressure indicator and temperature controller, respectively.

monitor the precipitation of gold particles with added CO_2 pressure. The cell had a stainless steel body with two O-ring sealed windows on opposite ends. The optical path length of the cell was 3 cm. A quartz cuvette of 10 mm path length was filled with 3 mL of organic solvent and 200 μL of the hexane solution of dispersed nanoparticles. A Teflon cuvette holder was then used to position the dispersion in a quartz cuvette at the centerline of the windows. The view cell was then pressurized with CO_2, using an ISCO 260D syringe pump, and UV−vis absorbance spectra were collected at each operating pressure until the maximum absorbance value reached a steady value. This was an indication of an equilibrium condition being reached in terms of particle dispersion.

Size-Selective Precipitation Process. The spiral tube apparatus as shown in Figure 1 was fabricated to obtain monodisperse metal nanoparticle populations[23] from an initially polydisperse population through precipitation at specific locations on a surface via CO_2 pressurization. This apparatus involves a 12 cm long, 2 cm diameter glass tube modified to include a concentric, spiral indentation on the surface of the tube from one end to the other. This indentation provides a 6 mm deep, 2.5 cm wide spiral channel, or groove, inside of the tube that allows a liquid droplet of nanoparticle dispersion resting within the channel to be translated from one location to another by a simple rotation of the tube while keeping the length of the tube horizontal. The spiral tube is situated within a cylindrical high-pressure stainless steel view cell equipped on one end with an O-ring sealed quartz window for observation. The other end is fitted with a Teflon tapered high-pressure fitting that allows entry of a 1/8 in. stainless steel rod attached to the spiral tube with a Teflon interconnect. This assembly allows radial rotation of the spiral tube within the high-pressure vessel by simply turning the metal rod from outside the vessel while a dynamic high-pressure seal is maintained by the Teflon fitting. The location of a liquid droplet situated in the glass tube channel (inside the tube) can then be controlled by turning the steel rod. The process was initiated by introducing 700 μL of pure hexane into the high-pressure view cell in the annular space outside of the spiral tube and allowing it to sit for at least 10 min. This hexane was introduced to saturate the system with hexane vapor prior to introducing the nanoparticle dispersion sample. This was done to minimize evaporative losses of hexane from the dispersion droplet during the separation process. Next, 250 μL of the hexane dispersion of thiol-coated metal particles was introduced into the channel of the spiral tube at the horizontal position closest to the quartz window as shown in the top image in Figure 2. The vessel was then slowly pressurized to an initial pressure of 550 psi and allowed 20 min to equilibrate at location

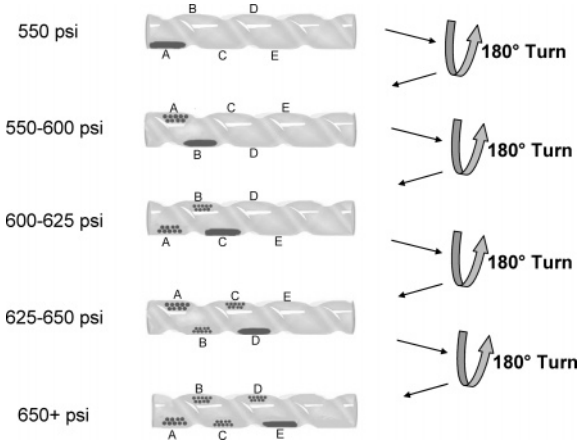

Figure 2. Nanoparticle size-selection spiral tube apparatus depicting recursive pressurization of organic liquid with CO_2, followed by 180° tube rotations to achieve multiple size-selected populations.

A in the spiral tube. Of the overall 950 μL of hexane introduced into the 60 mL vessel (both inside and outside of the spiral tube), 15% of this hexane is dissolved into the CO_2 gaseous phase at equilibrium at 500 psi and 25 °C, and this partitioning is increased to 22% of this hexane dissolved into the CO_2 at the highest pressure of 700 psi as determined by phase-equilibrium calculations using the Peng Robinson equation of state. More importantly, the increased concentration of CO_2 in the solvent mixture (liquid phase) decreases the overall solvent strength such that particles too large to be stabilized by the now weakened CO_2/solvent mixture will precipitate during the 20 min settling time.

Van der Waals forces cause the particles to adhere to the surface on which they precipitate. To separate the remaining liquid dispersion from the precipitated particles, the tube was rotated by turning the rod 180°. This rotation moves the liquid dispersion to the next location, B (180° around the tube, but further along axially), leaving behind the precipitated particles affixed to the spiral groove, at location A. The vessel was then pressurized to 600 psi with the suspension at the new location; the particles that precipitate at this pressure are, on average, smaller than those that precipitated at the lower pressure. The glass tube was then turned another 180° to take the dispersion to a new location C, leaving this second fraction of affixed particles behind in the second location B. This process was continued to acquire fractions at 625 and 650 psi at positions C and D, respectively. A final precipitation at 700 psi can induce the precipitation of the remaining particles from the hexane dispersion at location E in the spiral tube.

Sample Collection. After completing the final precipitation, the vessel was depressurized. There were five particle populations in the spiral tube at locations A, B, C, D, and E. These five particle samples were recovered through redispersion in hexane, giving five different size fractions. Sample grids were made by evaporative deposition and tested for particle size distribution on a Zeiss EM 10 Transmission Electron microscope (TEM).

Results and Discussion

Volume Expansion of the Solution. When a given organic dispersion of nanoparticles was pressurized with CO_2, the volume of the organic phase was increased by dissolution of CO_2 until equilibrium was reached. This increase in volume of the organic dispersion/CO_2 mixture can be characterized by the volume expansion coefficient, defined as $(V - V_0)/V_0$, where V

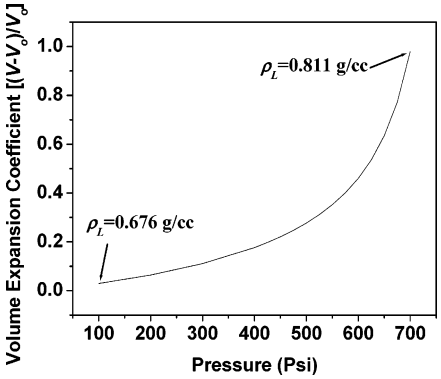

Figure 3. Volume expansion coefficient vs system pressure for liquid hexane/CO_2 mixtures pressurized with gaseous CO_2 and modeled with the Peng−Robinson equation of state at 25 °C.

is the volume of the solution saturated with CO_2 at a given pressure and V_0 is the volume of the CO_2-free solution (unpressurized). This volume expansion coefficient was estimated by using the Peng−Robinson equation of state[42] and compared well to measurements made by visual observation of volume expansion in a high-pressure Jerguson sight gauge (less than 5% error between the experimental data and the equation of state in the pressure range of 500 to 700 psi). This volume expansion coefficient is necessary when interpreting UV−visible spectra to compensate for the decrease in particle concentration that accompanies an increase in solution volume with CO_2 pressure. The volume expansion coefficient of hexane for a range of CO_2 pressures as determined by the Peng−Robinson equation of state is shown in Figure 3 where increases in CO_2 pressure significantly increase the volume expansion coefficient as a result of CO_2 gas partitioning into the liquid phase. Interestingly, this dissolution of CO_2 in the organic solvent also increases the density of the solvent mixture as obtained from the Peng−Robinson equation of state, indicating that while these mixtures are referred to as gas-expanded liquids, the resulting solution is a dense mixture of liquid CO_2 and organic solvent. However, CO_2 is a very poor solvent for the solvation of the ligand-coated particles in the organic solvent mixture. Therefore, as the percentage of CO_2 increases in the expanded organic solvent, solvent−ligand interactions decrease and the dispersed particles will precipitate once a threshold solvent strength is passed.

UV−Visible Absorbance Spectroscopy. An increase in CO_2 pressure decreases the concentration of dispersed nanoparticles. This is due to a decrease in the solvent strength of the GEL. Here, a decrease in solvent strength means that CO_2 has a very poor interaction with the n-alkyl ligand tails attached to the nanoparticles as compared to the organic solvent. So, as the concentration of CO_2 in the GEL is increased, interactions between the ligand tails and the solvent are diminished such that particles are no longer stabilized and start precipitating from the solvent. The precipitation of the nanoparticles from the organic solvent depends on many factors, such as ligand type, solvent type, temperature, and metal type. The effect of each of these variables on the nanoparticle precipitation process is examined in this paper.

Figure 4 presents the UV−vis spectra of gold particles synthesized by arrested precipitation and dispersed in hexane (top line). This absorption band is attributed to the absorption of Au nanoparticles dispersed in hexane and is due to the excitation of plasma resonances or interband transitions.[43] The gold nanoparticles do not precipitate in the absence of CO_2 even after extended periods of time. However, the intensity of the

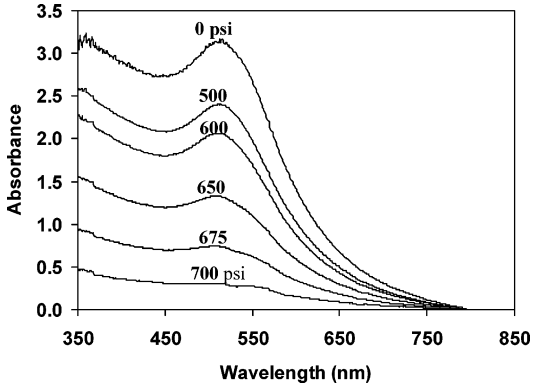

Figure 4. UV−visible absorbance spectra of gold particles dispersed in hexane/CO_2 liquid mixtures at increasing CO_2 pressures. The spectra were normalized to give zero absorbance at 800 nm wavelength. Decreased absorbance of gold particles after correcting for the volume expansion of hexane shows that particles are precipitating from hexane by increasing the CO_2 pressure.

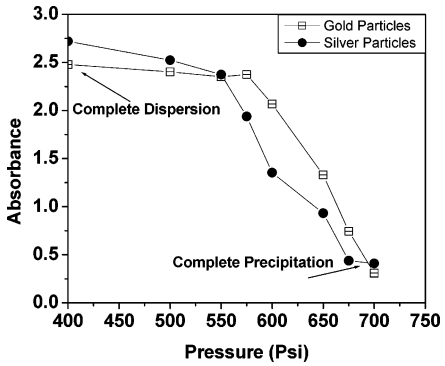

Figure 5. Maximum UV−visible absorbance of dodecanethiol coated silver[23] and gold particles dispersed in liquid hexane/CO_2 mixtures vs system pressure. Absorbance values obtained were corrected for the volume expansion of the liquid mixture.

UV absorbance band decreases when the nanoparticle dispersion was pressurized with CO_2. This decrease in intensity indicates that particles begin precipitating from solution and the absorbance maximum decreases with the increase in pressure. Correspondingly, the absorbance maxima of the UV−visible spectra, after correcting for the volume expansion of the organic solvent with the addition of CO_2, was plotted against the CO_2 pressure as a measure of particle concentration that remains dispersed at a given CO_2 pressure. Figure 5 shows a decrease of the absorbance with an increase in the pressure of CO_2 and indicates that the gold nanoparticles primarily precipitate from the solution in the range of 500 to 700 psi of CO_2 pressure. At pressures higher than 700 psi, complete precipitation occurs. The gold particles used in this experiment had a mean particle size of 5.0 nm and a standard deviation of 26% as shown in Table 1. McLeod et al.[23] also demonstrated a dramatic decrease in the UV absorbance band for dodecanethiol stabilized silver particles dispersed in hexane with similar increases in CO_2 pressure (also shown in Figure 5). The mean particle size and standard deviation for these silver particles[23] was 5.5 nm and 31.9%, respectively. Interestingly, the pressure range for the precipitation and the slope of this curve was very similar for both the gold and silver nanoparticles. This is consistent with the fact that both dodecanethiol stablizied gold[44] and dodecanethiol stabilized silver[14] nanoparticles have Hamaker constants of 1.95 eV resulting in similar inherent van der Waals forces of attraction.

TABLE 1: Statistical Analysis of Particle Populations Where the Five Fractions Were Separated in a Single Experiment from the Original Population[a]

fraction (psi)	ΔP of fraction (psi)	mean diameter (nm)	std dev (nm)	rel std dev (%)	95% confidence (nm)	particle count
original	0	5.0	1.3	26.0	0.1	534
0 to 550	555.0	5.7	1.3	22.4	0.1	594
550 to 600	50	5.5	0.9	15.9	0.07	556
600 to 625	25	4.8	0.6	12.5	0.05	522
625 to 650	25	4.3	0.5	11.0	0.04	459
650+	<50	3.4	0.7	20.6	0.06	579

[a] All gold particles are completely precipitated from the hexane at 700 psi.

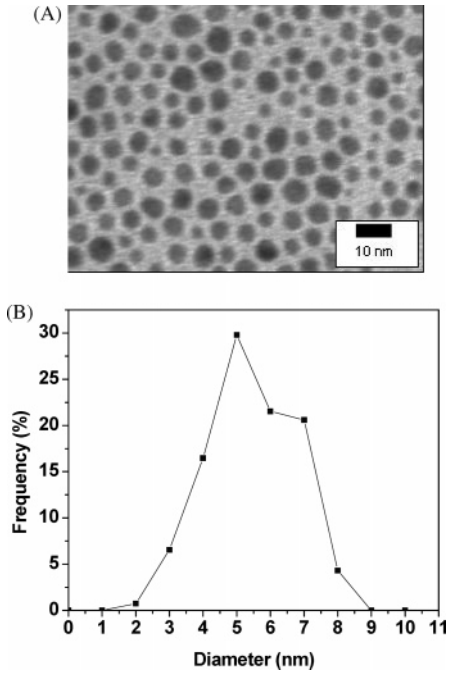

Figure 6. (A) TEM micrograph of unprocessed dodecanethiol-coated gold particles prepared by the two-phase arrested precipitation method. (B) Size distribution of unprocessed particles.

TEM Characterization. The particle size precipitated at each pressure range was determined by analysis of TEM images by using ImageJ software where each particle was bounded by a rectangle and the diameter was estimated by the average of the length and the width of the rectangle. Figure 6A shows an example of the TEM micrographs of unprocessed dodecanethiol-coated gold particles prepared by the two-phase arrested precipitation method as explained earlier. These images were analyzed to determine the size distribution of this original sample as shown in Figure 6B. This original sample of polydisperse dodecanethiol-coated gold particles was fractionated in a spiral tube into five fractions corresponding to different pressure ranges at different locations in the spiral tube as shown by arrows in Figure 7. TEM images of these fractions given in Figure 7 illustrate that the particle size collected within each ΔP decreases with increased CO_2 pressure. Moreover, particles in these images are very monodisperse and significantly more ordered into arrays as a result of the size-separation process. After analyzing these particles with ImageJ software, histograms were prepared for all five pressure ranges simultaneously as shown in Figure 8 to quantitatively compare the various fractions. Compared to the wide size distribution (Figure 6B) of the original sample ranging from 2 to 9 nm, the histograms of the distinct fractions obtained after the size-separation process are sharp (±2 nm). The size-separation process improves the quality of the particles by increasing the percentage of particles at the median particle size in a single experiment. For example, 30% of the original group of nanoparticles was 5 nm in diameter but after the size-separation process, 70% of the particles in the 650 psi fraction were 5 nm. Table 1 shows a statistical analysis of the fractions obtained at different pressure ranges from the size-selection process. The standard deviation of the original sample is 26%. At 550 psi, the standard deviation is 22.4% because the pressure range, ΔP for collection, is large (0 to 550 psi). The standard deviation was reduced to 15.9% for the particles precipitated from 550 to 600 psi with a ΔP of 50 psi. The standard deviation was further reduced to 12.5% at 625 psi and 11.0% at 650 psi with ΔP values of 25 psi in each of these fractionation steps. This illustrates that a smaller ΔP gives a more precise particle separation due to a more subtle change in solvent strength and the process can be manipulated to obtain a desired particle size. McLeod et al.[23] showed that pressure can be used as a parameter to obtain a desired particle size. McLeod et al. also showed that smaller pressure ranges (ΔP) for precipitation can be used to further narrow the size distribution where a ΔP of 50 psi resulted in a standard deviation of 16.1% and a ΔP of 6 psi resulted in a standard deviation of 14.7% for silver particles.

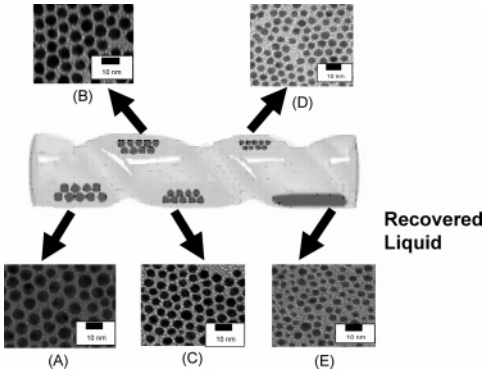

Figure 7. TEM micrographs of particles precipitated from hexane by CO_2 pressurization from (A) 0 to 550, (B) 550 to 600, (C) 600 to 625, (D) 625 to 650, and (E) 700 psi CO_2 pressurization.

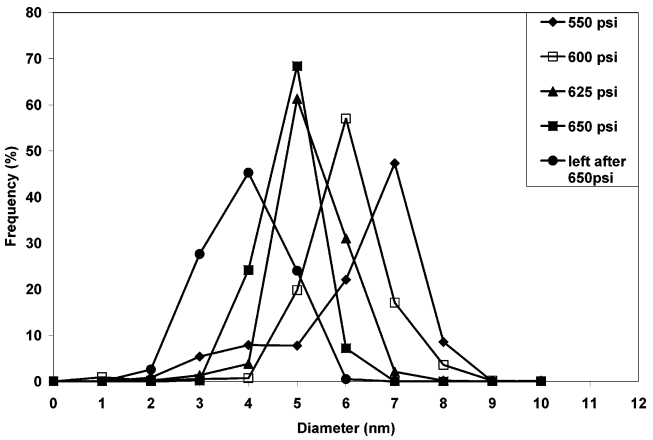

Figure 8. Size distributions of dodecanethiol-coated gold particles fractionated within the CO_2 pressure ranges of 0−550 (◆), 550−600 (□), 600−625 (▲), 625−650 (■), and 700 psi (●). Data points represent the percentage of particles of the total population found between the associated diameter and <1 nm less than that diameter.

Effect of Solvent Hydrocarbon Length on the Size-Selective Precipitation Process. Kitchens et al.[16] explained that variations in bulk solvent strength can have a significant effect on the size of nanoparticles that can be sterically stabilized in a given solvent. For example, cyclohexane solvent was shown

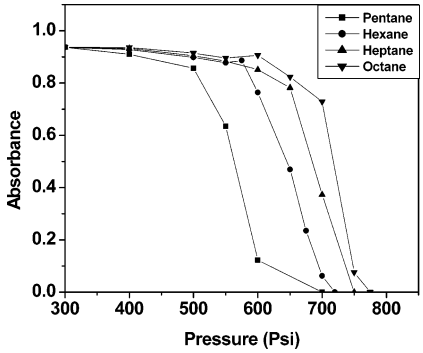

Figure 9. Maximum UV−visible absorbance values for dodecanethiol coated gold nanoparticles dispersed in different hydrocarbon length solvents pressurized with CO_2.

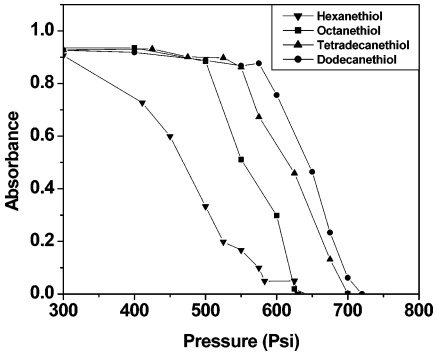

Figure 10. Maximum UV−visible absorbance values for gold nanoparticles coated with different thiol length molecules dispersed in liquid hexane/CO_2 mixtures at increasing CO_2 pressure.

to disperse larger AOT-stabilized copper nanoparticles than was hexane solvent at identical operating conditions as a result of stronger AOT−solvent interactions. Shah and co-workers also demonstrated that the dispersability of dodecanethiol stabilized gold and silver particles could be varied in liquid and supercritical ethane by altering the pressure and thereby tuning the solvent density.[28] Moreover, variations in solvent strength can play an important role in the precipitation and deposition[20,45] processes of particles. For example, Sigman and co-workers examined the morphology of dodecanethiol stabilized gold and silver nanocrystal thin films that were deposited from various solvents and they attributed the morphology changes to the different interparticle attractions in the organic solvents.[20] Rough superlattice films were obtained from hexane, while smooth films were deposited from chloroform. Each of these works demonstrate that the interactions between the solvent and the particle-stabilizing ligands play an important role in the dispersion and precipitation of nanoparticles. In general, a decrease in the solvent strength weakens the solvation of the ligand tails and results in stronger tail−tail interactions[46] thereby decreasing the particle dispersability. Sufficient solvation of the thiol stabilizing ligand tails is necessary to provide enough repulsive force (osmotic and elastic repulsion) to overcome the van der Waals forces of attraction between the nanoparticles.

The effect of different solvents on the size-selective precipitation and fractionation process was examined. Figure 9 presents maximum UV−visible absorbance values for dodecanethiol-coated gold nanoparticles dispersed in different hydrocarbon length solvents pressurized with CO_2. These absorbance maxima were normalized to a common initial value for ease of comparison and zero absorbance simply denotes that all the particles were precipitated from solution at that pressure. In hexane, a large percentage of the particles remained dispersed up to 550 psi after which point more appreciable precipitation occurred (precipitation of successively smaller particles) with further increases in CO_2 pressure until all the particles had precipitated at 700 psi and beyond. In contrast to hexane, pentane is a slightly weaker solvent, and as such, appreciable precipitation was initiated at only 450 psi with complete precipitation as low as 600 psi. Given that pentane provides weaker solvation of the ligand tails than hexane, smaller amounts of CO_2 are necessary to bring the solvent/CO_2 mixture solvent strength below the threshold for dispersability of a given particle size. As a result, the pressure range required for precipitation is less in pentane than in hexane. Interestingly, heptane and octane both exhibit stronger interactions with the ligand tails as compared to hexane resulting in more stable dispersions in the longer chain length solvents. Correspondingly, greater CO_2 pressure is required to reach the same weakened solvent strength of the solvent/CO_2 mixture to induce precipitation of nanoparticles of a given size. Figure 9 shows that the length of the organic solvent influences the gold nanoparticle precipitation process where the longer length solvent molecules have stronger interactions with the nanoparticle ligand tails compared to the shorter length solvent molecules. Additional results of similar experiments performed with cyclohexane, decane, isooctane, and toluene are not shown here in Figure 9. In these solvent systems, particle dispersability remained quite high even at CO_2 pressures approaching the vapor pressure of CO_2 where the dodecanethiol-coated gold particles remained dispersed in the solvent/CO_2 mixtures for several hours.

Effect of Thiol Length on the Size-Selective Precipitation Process. Martin et al.[47] states that among all the alkanethiols, dodecanethiol is more strongly bound to gold particles than hexanethiol or hexadecanethiol. Prasad et al.[44] studied the effect of the alkyl chain lengths of thiol molecules on the formation of gold nanoparticle superlattices. These authors describe that there is a decrease in particle−particle attraction energy with an increase in the thiol hydrocarbon chain length. For example, particles aggregated into 3D superlattices with short chain lengths, i.e., octanethiol and decanethiol (C_8 and C_{10}), due to particle−particle attraction. The longer chain length in hexadecanethiol resulted in weakly bound multilayers and hinders the development of 3D superlattices. These works have demonstrated the impact of thiol chain length on particle−particle attraction. It is important to note that in the current study, dispersion of particles in solution requires that these attractive interactions be finely balanced by the osmotic repulsion and an elastic contribution generated by interactions between the solvent and the thiol stabilizing ligands. As shown in the previous section of this paper, modification of the solvent strength of the solution (i.e., CO_2 pressurization) can result in changes in these attractive and repulsive interactions thereby inducing precipitation. Changes in this fine balance can also be accomplished by altering the thiol chain length such that there is a modification to the interaction between the solvent and the thiol ligand tails. Here we present the influence of various thiol chain lengths on the CO_2 pressurization range required to induce precipitation. As shown in Figure 10, precipitation of the particles stabilized with octanethiol ligands occurs between 400 and 600 psi as compared to 500−700 psi for particles stabilized by dodecanethiol ligands. The precipitation of particles with hexanethiol ligands was similar to those with octanethiol ligands, and the curve was shifted to a lower pressure range (300−575 psi). Particles stabilized with tetradecanethiol ligands require a smaller CO_2 pressure for the precipitation of particles compared to dodecanethiol ligands, even though they have a longer tail length. The shorter tail length for octanethiol and hexanethiol

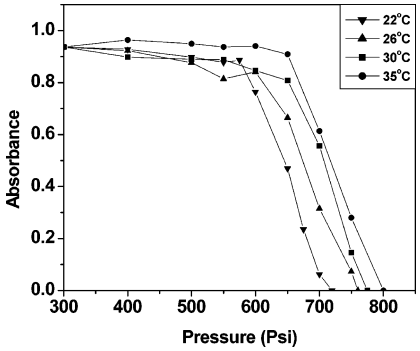

Figure 11. Maximum UV−visible absorbance values for dodecanethiol coated gold nanoparticles dispersed in liquid hexane/CO_2 mixtures at various CO_2 pressures and system temperatures.

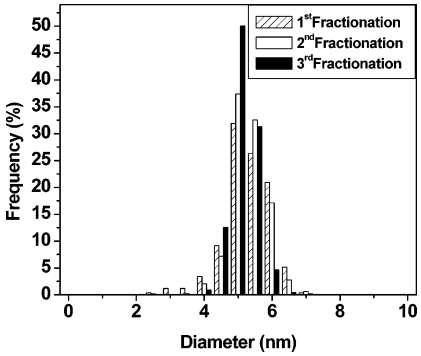

Figure 12. Comparison between the size distributions of dodecanethiol coated gold particles collected in the pressure range of 625 to 650 psi after fractionation one, two, or three times. Particles from the 1st fractionation were obtained from location D in the spiral tube apparatus corresponding to a pressure range of 625−650 psi. This 1st fractionation sample was returned to location A and the size-separation process was repeated. The 2nd fractionation sample was again obtained from position D. In the same way, the 3rd fractionation was obtained by placing the 2nd fractionation sample at location A and collecting the particles precipitated at location D. Data points represent the percentage of particles of the total population found between the associated diameter and <0.5 nm less that the diameter.

ligands decreases the CO_2 pressure required for precipitation in a GEL compared to dodecanethiol ligand-stabilized particles. This effect is because the shorter length ligands have smaller interactions with the solvent compared to the longer length ligands. Tetradecanethiol ligand-stabilized particles also require less CO_2 pressure for the nanoparticle precipitation than dodecanethiol ligand-stabilized particles. These results suggest that dodecanethiol ligands have the optimum length for strong ligand−solvent interactions.[44]

Effect of Temperature on the Size-Selective Precipitation Process. Temperature also has a pronounced effect on nanoparticle stabilization and dispersibility.[16] As shown by Shah and co-workers,[28] temperature affects solvent density, which affects the nanoparticle dispersability in an organic solvent. Temperature effects on the precipitation of gold particles stabilized with dodecanethiol ligands in hexane are shown in Figure 11. At the lowest temperature of 22 °C, the nanoparticle precipitation occurs between 500 and 700 psi CO_2 pressure. At the highest temperature of 35 °C, this pressure range for precipitation was shifted up to 650 to 800 psi, illustrating that an increase in pressure is required for precipitation with an increase in temperature. This variation is due in part to the CO_2 density change with temperature. As temperature is increased, the mole fraction of CO_2 in the organic liquid/CO_2 mixture is reduced resulting in a smaller volume expansion of the liquid dispersion at a given pressure. This, therefore, reduces the antisolvent effect in the nanoparticle precipitation process.

Recursive Fractionations. Korgel and co-workers used ethanol recursively as an antisolvent to improve the size-separation process.[20] In the current study, a set of size-separation experiments were repeated on one of the recovered fractions (particles collected within a given pressure range at one location in the spiral tube) to further improve the size-separation process with CO_2 as an antisolvent. The results of the recursive fractionation are summarized in Figure 12. The size-separation process, shown in Figure 2, was done by placing the original polydisperse sample at location A in the spiral tube. The 1st fractionation sample, at location D, shown in Figure 12 was the sample of particles precipitated within the pressure range of 625−650 psi. In this recursive process, this 1st fractionation sample was collected in hexane at the end of the experiment and was returned to location A and the size-separation process was repeated. The 2nd fractionation sample shown in Figure 12 was again obtained from position D within the same pressure range of 625−650 psi. In the same way, the 3rd fractionation was obtained by placing the 2nd fractionation sample at location A and collecting the particles precipitated at location D within the same pressure range. The separation was improved during each successive processing step with a decrease in the standard deviation from 13% to 8% as shown in Table 2. Of course the standard deviation could be further reduced by continuing the recursive fractionation steps or by initiating the process with a less polydisperse initial sample. The sample shown here involved a highly polydispersed initial sample to illustrate that a range of particle sizes can be fractionated. This process is an improvement over the liquid antisolvent process where the desired size is controllably obtained as a function of pressure. For instance, keeping the solvent, thiol length, and temperature the same, this process will always result in a ∼5.0 nm sized fraction of gold particles collected at 650 psi since the precipitation is governed simply by the solvent strength. Therefore, this CO_2 antisolvent size-separation process gives a predictable particle size at a given CO_2 pressure. On the other hand, the number of variables involved in the liquid antisolvent process including the specific amount of ethanol addition and the centrifugation time makes predictable size selection challenging.

TABLE 2: Statistical Analysis of Particle Populations for Different Numbers of Fractionations

fractionation (no.)	mean diameter (nm)	std dev (nm)	rel std dev (%)	fraction (psi)	95% confidence (nm)	particle count
1	5.0	0.7	13.1	625−650	0.06	502
2	5.0	0.5	10.0	625−650	0.04	642
3	4.9	0.4	8.1	625−650	0.04	454

Effect of Time on the Size-Selective Precipitation Process. During this size-selection process, the liquid droplet with dispersed nanoparticles is moved to a specific location on the surface of the spiral tube followed by an increase in pressure that initiates precipitation of particles within that pressure range. Once the desired pressure is reached, the system is allowed to sit for a specified period of time allowing precipitation of the particles, and this period of time is referred to as the holding time. Table 3 presents standard deviations for particles precipitated during three different holding times in the pressure range of 600−625 psi. The results shown earlier in this paper were collected during a holding time of 20 min where a mean size of 4.7 nm and a standard deviation of 14.9% were obtained as given in Table 3. For a holding time of 1 h, the mean size and standard deviation were 4.7 nm and 16.9%, respectively. It was

TABLE 3: Statistical Analysis of Particle Populations for Different Holding Times

holding time (min)	mean diameter (nm)	std dev (nm)	rel std dev (%)	95% confidence (nm)	particle count	fraction (psi)
5	5.1	0.75	14.6	0.06	464	600 to 625
20	4.7	0.70	14.9	0.07	309	600 to 625
60	4.7	0.79	16.9	0.06	591	600 to 625

found that a 5 min holding time resulted in a standard deviation of 14.6% with a mean nanoparticle size of 5.1 nm. The experiments performed at different holding times suggest that there is little difference in the size distribution of the nanoparticles collected. This demonstrates that the size-separation process with CO_2 as the antisolvent is a very rapid process compared to the liquid antisolvent process that requires several hours for the separation of the same quantity of particles.

Conclusions

A method for precise, rapid, pressure-tunable, size-selective nanoparticle precipitation and redispersion with tunable CO_2 gas-expanded liquids has been developed. This technique is a marked improvement over the current techniques of nanoparticle fractionation employing liquid antisolvent techniques. In this size-separation process, dodecanethiol stabilized polydisperse gold nanoparticles dispersed in hexane were fractionated into monodisperse fractions using CO_2 pressurization in the range of 500−700 psi. The original sample of dodecanethiol-stabilized gold particles of 26% polydispersity were successfully separated into fractions of as little as 11% polydispersity in a single-step process. To understand the precipitation process in more detail, the effect of various parameters on the size-separation process was studied. Variations in solvent length from five to eight hydrocarbon chains have a significant effect on the pressures required for precipitation of dodecanethiol-coated gold nanoparticles. Experiments in which the thiol stabilizing ligand length was varied illustrated that dodecanethiol provides the best solvent−ligand tail interaction when hexane was the bulk solvent medium. It was also found that as the solvent temperature was increased, an increase in CO_2 pressure is required to completely precipitate all the nanocrystals from solution. Recursive fractionations on a sample collected within a given pressure range elicit the desired nanoparticles of a precise size. This new process is very fast, repeatable, and reproducible requiring a very short holding time at each precipitation stage.

Acknowledgment. The authors thank the Department of Energy Basic Energy Sciences (DE-FG02-01ER15255) for financial support of this work. The authors also thank James Osborn and Dr. Juncheng Liu for their technical assistance and helpful discussions.

References and Notes

(1) Poole, C. P. J.; Owens, F. J. *Introduction to Nanotechnology*; Wiley-Interscience: Hoboken, NJ, 2003.

(2) Pal, B.; Torimoto, T.; Iwasaki, K.; Shibayama, T.; Takahashi, H.; Ohtani, B. *J. Phys. Chem. B* **2004**, *108*, 18670.

(3) Maillard, F.; Schreier, S.; Hanzlik, M.; Savinova, E. R.; Weinkauf, S.; Stimming, U. *Phys. Chem. Chem. Phys.* **2005**, *7*, 385.

(4) Arenz, M.; Mayrhofer, K. J. J.; Stamenkovic, V.; Blizanac, B. B.; Tomoyuki, T.; Ross, P. N.; Markovic, N. M. *J. Am. Chem. Soc.* **2005**, *127*, 6819.

(5) Nakashima, P. N. H.; Tsuzuki, T.; Johnson, A. W. S. *J. Appl. Phys.* **1999**, *85*, 1556.

(6) Mahamuni, S. *Solid State Phys., Proc. DAE Solid State Phys. Symp., 41st., 1998* **1999**, 33.

(7) Bruchez, M., Jr.; Moronne, M.; Gin, P.; Weiss, S.; Alivisatos, A. P. *Science* **1998**, *281*, 2013.

(8) Drachev, V. P.; Buin, A. K.; Nakotte, H.; Shalaev, V. M. *Nano Lett.* **2004**, *4*, 1535.

(9) Valden, M.; Lai, X.; Goodman, D. W. *Science* (*Washington, D.C.*) **1998**, *281*, 1647.

(10) Haruta, M. *Catal. Today* **1997**, *36*, 153.

(11) Stowell, C.; Korgel, B. A. *Nano Lett.* **2001**, *1*, 595.

(12) Shah, P. S.; Sigman, M. B., Jr.; Stowell, C. A.; Lim, K. T.; Johnston, K. P.; Korgel, B. A. *Advanced Materials*; Wiley: Weinheim, Germany, 2003; Vol. 15, p 971.

(13) Shah, P. S.; Novick, B. J.; Hwang, H. S.; Lim, K. T.; Carbonell, R. G.; Johnston, K. P.; Korgel, B. A. *Nano Lett.* **2003**, *3*, 1671.

(14) Korgel, B. A.; Fullam, S.; Connolly, S.; Fitzmaurice, D. *J. Phys. Chem. B* **1998**, *102*, 8379.

(15) Cason, J. P.; Roberts, C. B. *J. Phys. Chem. B* **2000**, *104*, 1217.

(16) Kitchens, C. L.; McLeod, M. C.; Roberts, C. B. *J. Phys. Chem. B* **2003**, *107*, 11331.

(17) Brust, M.; Walker, M.; Bethell, D.; Schiffrin, D. J.; Whyman, R. *J. AM. Chem. Soc.* **1994**, *116*, 801.

(18) Murray, C. B.; Kagan, C. R.; Bawendi, M. G. *Annu. Rev. Mater. Sci.* **2000**, *30*, 545.

(19) Murray, C. B.; Norris, D. J.; Bawendi, M. G. *J. Am. Chem. Soc.* **1993**, *115*, 8706.

(20) Sigman, M. B., Jr.; Saunders, A. E.; Korgel, B. A. *Langmuir* **2004**, *20*, 978.

(21) Arnaud, I.; Abid, J.-P.; Roussel, C.; Girault, H. H. *Chemical Communications (Cambridge, UK)* **2005**, 787.

(22) Siebrands, T.; Giersig, M.; Mulvaney, P.; Fischer, C. H. *Langmuir* **1993**, *9*, 2297.

(23) McLeod, M. C.; Anand, M.; Kitchens, C. L.; Roberts, C. B. *Nano Lett.* **2005**, *5*, 461.

(24) Shah, P. S.; Hanrath, T.; Johnston, K. P.; Korgel, B. A. *J. Phys. Chem. B* **2004**, *108*, 9574.

(25) Shah, P. S.; Husain, S.; Johnston, K. P.; Korgel, B. A. *J. Phys. Chem. B* **2002**, *106*, 12178.

(26) Kitchens, C. L.; Roberts, C. B. *Ind. Eng. Chem. Res.* **2004**, *43*, 6070.

(27) Clarke, N. Z.; Waters, C.; Johnson, K. A.; Satherley, J.; Schiffrin, D. J. *Langmuir* **2001**, *17*, 6048.

(28) Shah, P. S.; Holmes, J. D.; Johnston, K. P.; Korgel, B. A. *J. Phys. Chem. B* **2002**, *106*, 2545.

(29) Liu, D.; Zhang, J.; Han, B.; Chen, J.; Li, Z.; Shen, D.; Yang, G. *Colloids Surf., A* **2003**, *227*, 45.

(30) Zhang, J.; Han, B.; Liu, J.; Zhang, X.; He, J.; Liu, Z.; Jiang, T.; Yang, G. *Chemistry−A Eur. J.* **2002**, *8*, 3879.

(31) Zhang, J.; Han, B.; Liu, J.; Zhang, X.; Yang, G.; Zhao, H. *J. Supercrit. Fluids* **2004**, *30*, 89.

(32) Wei, M.; Musie, G. T.; Busch, D. H.; Subramaniam, B. *J. Am. Chem. Soc.* **2002**, *124*, 2513.

(33) Thomas, C. A.; Bonilla, R. J.; Huang, Y.; Jessop, P. G. *Can. J. Chem.* **2001**, *79*, 719.

(34) Xie, X.; Liotta, C. L.; Eckert, C. A. *Ind. Eng. Chem. Res.* **2004**, *43*, 7907.

(35) Gallagher, P. M.; Coffey, M. P.; Krukonis, V. J.; Klasutis, N. *ACS Symp. Ser.* **1989**, *406*, 334.

(36) Eckert, C. A.; Bush, D.; Brown, J. S.; Liotta, C. L. *Ind. Eng. Chem. Res.* **2000**, *39*, 4615.

(37) Chen, J.; Zhang, J.; Liu, D.; Liu, Z.; Han, B.; Yang, G. *Colloids Surf.* **2004**, *33*, 33.

(38) Xie, X.; Brown, J. S.; Joseph, P. J.; Liotta, C. L.; Eckert, C. A. *Chem. Commun.* (*London*) **2002**, 1156.

(39) Jessop, P. G.; Olmstead, M. M.; Ablan, C. D.; Grabenauer, M.; Sheppard, D.; Eckert, C. A.; Liotta, C. L. *Inorg. Chem.* **2002**, *41*, 3463.

(40) Randolph, T. W.; Randolph, A. D.; Mebes, M.; Yeung, S. *Biotechnol. Prog.* **1993**, *9*, 429.

(41) Beckman, E. J. *Ind. Eng. Chem. Res.* **2003**, *42*, 1598.

(42) Peng, D.-Y.; Robinson, D. B. *Ind. Eng. Chem. Fundam.* **1976**, *15*, 59.

(43) Creighton, J. A.; Eadon, D. G. *J. Chem. Soc., Faraday Trans.* **1991**, *87*, 3881.

(44) Prasad, B. L. V.; Stoeva, S. I.; Sorensen, C. M.; Klabunde, K. J. *Langmuir* **2002**, *18*, 7515.

(45) McLeod, M. C.; Kitchens, C. L.; Roberts, C. B. *Langmuir* **2005**, *21*, 2414.

(46) Lee, C. T., Jr.; Johnston, K. P.; Dai, H. J.; Cochran, H. D.; Melnichenko, Y. B.; Wignall, G. D. *J. Phys. Chem. B* **2001**, *105*, 3540.

(47) Martin, J. E.; Wilcoxon, J. P.; Odinek, J.; Provencio, P. *J. Phys. Chem. B* **2000**, *104*, 9475.